Comparison of Theory and Experiment for Dispersion-Managed Solitons in a Recirculating Fiber Loop

R.-M. Mu, V. S. Grigoryan, Curtis R. Menyuk, *Fellow, IEEE,* G. M. Carter, *Senior Member, IEEE,* and J. M. Jacob

***Abstract*—We have developed a model that accurately predicts the dynamics of the signal pulses and the growth of amplified spontaneous emission noise in a dispersion-managed soliton pulse train propagating in a recirculating fiber-loop experiment. Theoretically predicted dependencies of the amplitude and phase margins for the marks and the amplitude margin for the spaces as a function of distance are in remarkable agreement with the experiments. This model allows us to determine the key physical effects that limit the propagation distance in our experiments.**

***Index Terms*—Amplitude margin, amplified spontaneous emission noise, dispersion-managed soliton (DMS), excess gain, filter, phase margin, pulse dynamics, timing jitter.**

I. Introduction

THE use of dispersion management has revolutionized the field of soliton transmission, resulting in record distances for single-channel transmission at 10 Gb/s [1], 20 Gb/s [2], and 40 Gb/s [3] without using stronger soliton controls. The advantages of the dispersion-managed soliton (DMS) over a standard soliton with the same bandwidth are attributed to an increase in signal power and a reduction of timing jitter relative to a transmission line that has a constant dispersion equal to the average value of the dispersion map [4]–[11]. A number of important factors that affect the performance of a communication system based on DMS pulses have been separately considered, including details of the dispersion map, the interaction between the signal and the noise, the nonlinear interaction between two signal pulses, and chromatic dispersion [12]–[21]. However, it is difficult to use this work to analyze or optimize a real experimental implementation of a DMS system because in any real system these effects occur simultaneously and interact with each other. The purpose of this paper is to overcome this limitation and present a complete model of a DMS transmission system that contains the essential physics needed to accurately model the data obtained from an experimental DMS system. With this model we were able to successfully reproduce the signal dynamics, including its transient evolution, the signal and noise variation with propagation distance, the timing jitter, the eye diagrams, and the bit-error rates (BER's) that were obtained in our experiments. In addition, we were able to identify the key limitations on propagation distances in our system based on the knowledge we gained through this investigation. This type of model will be beneficial for designing and optimizing system performance in non-DMS systems as well.

This paper is organized as follows. The model is developed in Section II. The dynamics of the signal propagation is presented in Section III. The growth of amplified spontaneous emission (ASE) noise and its impact on system performance are discussed in Section IV. Finally, Section V contains the conclusion.

II. Model and System Parameters

Our simulation model uses a modified nonlinear Schrödinger (NLS) equation that may be written as

$$i\frac{\partial q}{\partial z}+\frac{1}{2}\left[D(z)-ib(z)\right]\frac{\partial^2 q}{\partial t^2}+\frac{i}{6}d(z)\frac{\partial^3 q}{\partial t^3}+|q|^2 q = ia(z)q+\hat{F}(z,t). \tag{1}$$

Here, the pulse envelope q is normalized as $q = E(n_2\omega_0 L_D/A_{\text{eff}}c)^{1/2}$, where E is the electric field envelope, $n_2 = 2.6\times10^{-16}$ cm^2/W is the Kerr coefficient, ω_0 is the central frequency, $A_{\text{eff}} = 47$ μm is the effective area, and c is the speed of light. The quantity L_D is the characteristic dispersion length; it equals $T_0^2/|\beta_0''|$, where T_0 is a characteristic scale time, and β_0'' is the dispersion that we used to normalize the NLS and is set to 1.2 ps/nm·km. In our simulation, we chose $T_0 = 5.67$ ps, which roughly equals the root-mean-square soliton duration at the points of maximum compression. The distance z is normalized as $z = Z/L_D$, where Z is the physical distance along the recirculating loop. It increases continually as the signal undergoes multiple turns in the loop. The retarded time t is normalized as $t = (T-\beta_0' Z)/T_0$, where T is the physical time and β_0' is the inverse group velocity. Other quantities are normalized as follows: $D(z) = -\beta''(z)/|\beta_0''|$, $d(z) = -\beta_0'''(z)T_0/|\beta_0''|$, where β_0''' is the third-order dispersion, $b(z) = B(z)L_D/T_0^2$, where $B(z)$ is the filter curvature,

Manuscript received May 3, 1999; revised September 21, 1999. This work was supported by NSF, DOE, and AFOSR.

R.-M. Mu is with the Department of Computer Science and Electrical Engineering, University of Maryland Baltimore County, Baltimore, MD 21250 USA (e-mail: mu@umbc.edu).

V. S. Grigoryan was with the Department of Computer Science and Electrical Engineering, University of Maryland Baltimore County, Baltimore, MD 21250 USA. He is now with Corvis Corporation, Columbia, MD 21046 USA.

C. R. Menyuk is with the Department of Computer Science and Electrical Engineering, University of Maryland Baltimore County, Baltimore, MD 21250 USA. He is also with the Laboratory for Telecommunication Sciences, c/o: U.S. Army Research Laboratory, Adelphi Laboratory Center, Adelphi, MD 20783-1197 USA.

G. M. Carter is with the Department of Computer Science and Electrical Engineering, University of Maryland, Baltimore, MD 21250 USA. They are also with the Laboratory for Physical Sciences, College Park, MD 20740 USA.

J. M. Jacob was with the Department of Computer Science and Electrical Engineering, University of Maryland Baltimore County, Baltimore, MD 21250 USA. He is now with MCI WorldCom, Richardson, TX 75082 USA.

Publisher Item Identifier S 1077-260X(00)03439-0.

and $a(z) = \alpha(z)/2L_D$, where $\alpha(z)$ is the power gain or loss. The net gain coefficient $a(z)$ may be written as

$$a(z) = \begin{cases} g_m, & z_{m,r} < z < z_{m,r} + L_{\text{amp}} \\ -\Gamma, & \text{elsewhere} \end{cases} \tag{2}$$

where

- g_m is the gain coefficient of the mth amplifier;
- Γ is the loss coefficient of the fiber;
- $z_{m,r}$ is the initial position of the mth amplifier on the rth round-trip;
- L_{amp} is the amplifier length.

The autocorrelation function for the Langevin term in $F(z, t)$ (1) may be written as

$$\langle \hat{F}(z, t)\hat{F}^*(z', t')\rangle = 2\theta(z)g_m \frac{n_2\hbar\omega_0^2 L_D}{A_{\text{eff}}T_0 c}\,\delta(z - z')\delta(t - t') \tag{3}$$

where $\hbar$ is the Planck's constant and $\theta(z)$ equals the spontaneous emission factor n_{sp} when $z_{m,r} < z < z_{m,r} + L_{\text{amp}}$ and is zero elsewhere.

In order to accurately calculate the evolution of the DMS pulses in the recirculating loop, it is of critical importance to carefully calculate the effects of the amplifier saturation. We will return to this issue in more detail in Section III and confine our discussion here to presenting our modeling approach. Since the amplifier gain evolves on a time-scale of milliseconds, while $q(z, t)$ evolves on a time-scale of picoseconds, we must use a multiple time/length-scale approach in which we average over the rapid variations of $q(z, t)$ to determine the evolution of the gain and then fix the gain to determine the evolution of $q(z, t)$ [22]. If we consider the evolution of the gain coefficient of the mth amplifier in the loop, then its gain coefficient may be written

$$\frac{\partial g_m(\zeta, \tau)}{\partial \tau} + \frac{g_m(\zeta, \tau) - g_{m,0}}{\tau_A} = -\frac{g_m(\zeta, \tau)|q(\zeta, \tau)|^2}{U_{\text{sat}}} \tag{4}$$

where $\tau = T/T_0$ is the normalized time; in contrast to t used in (1), τ is unretarded. The distance ζ is internal to the amplifier so that $0 \le \zeta \le L_{\text{amp}}$ and is normalized with respect to L_D. The quantity $g_{m,0}$ is the unsaturated gain of the mth amplifier, τ_A is the normalized relaxation time, which, in physical units, we set equal to 1 ms, and U_{sat} is the saturation energy, which, in physical units, we set to 10 μJ, corresponding to a saturation power of 10 mW.

To solve (1) in parallel with (4), we must relate ζ and τ to z and t. To do so, we note that as the signal propagates along the loop, so that z is increasing, the time τ increases in the mth amplifier. Thus, we find that $\tau = (L_D\beta_0'/T_0)z$. The recirculating loop is a bit over 100-km long, so that a signal undergoes approximately two round-trips in one excitation time. Thus, we must take into account the transient evolution of the gain in each amplifier, as well as the variation of $|q(\zeta, \tau)|^2$ as a function of position ζ inside the amplifier. However, we may assume that at a fixed value of ζ, this variation is very slow. Since we only keep a limited range of τ in (1)—on the order of several hundred picoseconds—we may average over the rapid variations of $q(z, t)$ as a function of t to find

$$g_{m,r+1}(\zeta) = g_{m,r}(\zeta)\exp\left[-N\left(\frac{\Delta t}{\tau_A} + \frac{U_{m,r}(\zeta)}{U_{\text{sat}}}\right)\right] + g_{m,0}\frac{\Delta t}{\tau_A}\frac{1 - \exp\left[-N\left(\frac{\Delta t}{\tau_A} + \frac{U_{m,r}(\zeta)}{U_{\text{sat}}}\right)\right]}{\frac{\Delta t}{\tau_A} + \frac{U_{m,r}(\zeta)}{U_{\text{sat}}}} \tag{5}$$

where N pulses fill the loop with pulses separated in time by Δt so that $\Delta z = (T_0/L_D\beta_0')N\Delta t$ is one round-trip in the loop in normalized units. The integer r indicates the number of round-trips so that

$$g_{m,r}(\zeta) = g_m[\tau = (L_D\beta_0'/T_0)z_{m,r}, \zeta]. \tag{6}$$

Finally, the energy $U_{m,r}(\zeta) = \langle|q(z_{m,r} + \zeta, t)|^2\rangle\Delta t$ corresponds to the average energy in a single bit at $z = z_{m,r} + \zeta$. Having at each ζ determined the slow variation of the gain from (5), we then determine the fast variation of $q(z, t)$ from (1) by assuming that the gain is independent of t on each round-trip. We have found that dividing the amplifier into 100 sections yields a sufficiently accurate numerical solution for $g_{m,r}(\zeta)$. We note that in steady state, (5) becomes

$$g_{m,r+1}(\zeta) = g_{m,r}(\zeta) = \frac{g_{m,0}}{1 + \frac{\tau_A}{\Delta t}\frac{U_{m,r}(\zeta)}{U_{\text{sat}}}} \tag{7}$$

where $U_{m,r}(\zeta)$ is constant as a function of r. However, to obtain accurate results for the convergence of initial pulse shapes to their final values, one must use (5) rather than (7).

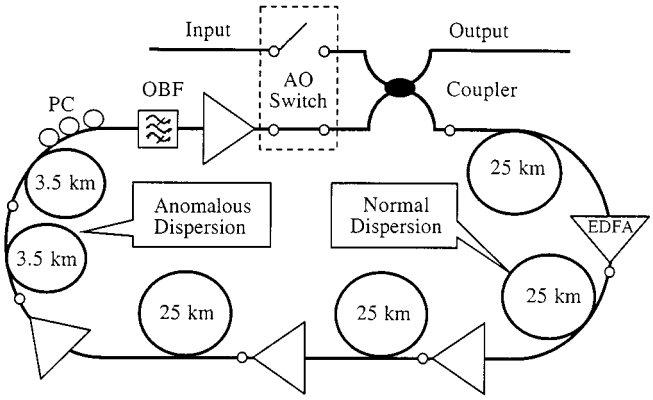

Fig. 1. The experimental setup. Small circles along the loop show the tap points at which experimental data could be extracted.

Fig. 1 shows our recirculating loop configuration [1]. There are four spans of dispersion-shifted fiber (SMF-LS), each about 25 km in length, with a normal dispersion D_1 equal to -1.10 ps/nm–km at 1551 nm, followed by an approximately 7-km span of standard single-mode fiber (SMF-28) with an anomalous dispersion D_2 equal to 16.6 ps/nm–km at 1551 nm.

TABLE I
FIBER PARAMETERS FOR CALCULATING DISPERSION

	D'_e	λ_0	L
	ps/nm^2-km	nm	km
SMF-28	0.088	1312	6.71
SMF-LS1	0.081	1565	25.059
SMF-LS2	0.080	1565	25.060
SMF-LS3	0.074	1566	25.058
SMF-LS4	0.069	1566	25.060

To calculate the dispersion as a function of wavelength we used the formulas

$$D(\lambda) = \frac{D'_e}{4}\left(\lambda - \frac{\lambda_0^4}{\lambda^3}\right) \quad \text{for SMF-28 fiber}$$

$$D(\lambda) = D'_e(\lambda - \lambda_0) \quad \text{for SMF-LS fiber}$$

on the data sheet that Corning Inc. provided along with the fiber that we purchased [23]. The quantity D'_e corresponds to an effective dispersion slope coefficient, while λ_0 corresponds to the zero-dispersion wavelength. We show the values of D'_e, λ_0, and the exact lengths of each fiber in Table I. The average dispersion slope over one loop period is about 0.075 ps/nm^2–km. By changing the central wavelength of the input signal, we were able to adjust the average dispersion $D_{\rm av}$. An amplifier follows each span of normal dispersion fiber and a fifth amplifier follows the 2.8-nm bandpass filter that is at the end of the 7 km span of standard fiber. The total loss within one loop period is 31.53 dB, including the loss in the fibers, the optical filter, connectors, couplers, and acoustio-optic switches. We also defined the total unsaturated gain coefficient within one loop period as

$$G_0 = \exp\left[\sum_{m=1}^{5}\left(2\int_0^{L_{\rm amp}} g_{m,0}\,dz\right)\right]$$

that can be altered by changing the individual unsaturated gain coefficient $g_{m,0}$ at each amplifier. In our investigation, we always set $\exp(2g_{m,0}L_{\rm amp}) = G_{a,0}$, $(m = 1 \cdots 4)$ the same and set $\exp(2g_{5,0}L_{\rm amp}) = G_{b,0}$ a little larger in order to compensate for the loss in the switches, the optical filter, and the couplers. The value of G_0 will determine the energy of the DMS pulse at steady state.

We now specify the initial condition in our simulations. Unless otherwise stated, we launched Gaussian-shaped pulses with a full-width at half maximum (FWHM) pulse duration of 9 ps and a peak power of 9 dBm at the midpoint of the anomalous span. The pulse train takes the form of 1-1-1-0-0-0-1-0, which includes all possible nearest-neighbor interactions since only the nearest-neighbor interactions are important for single-channel DMS systems. The bits were spaced 100 ps apart, corresponding to a 10 Gb/s signal. We used the split-step Fourier method to solve (1) with an 800-ps calculation window, so that the pulse train that we used is, in effect, repeated periodically *ad infinitum*.

Equations (1)–(5), along with the initial condition just specified, comprise the model of our recirculating loop experiments. The model will illustrate the principal characteristics of single-channel DMS in a communication system. The important characteristics are the nonlinear pulse propagation in the map, the accumulation of ASE noise, the interaction of the signal and the ASE noise, and the nonlinear interaction between adjacent pulses. In the following sections, we will illustrate how these coupled effects determine the system performance of our experimental system.

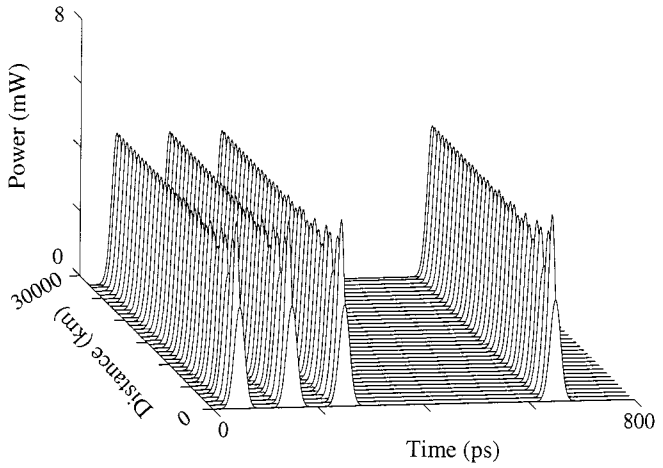

Fig. 2. The evolution of the DMS pulse trains as a function of the distance with $D_{\rm av} = 0.02$ ps/nm–km. In this case, we set $G_{a,0} = 5.4$ dB and $G_{b,0} = 10.85$ dB.

III. DYNAMICS OF DISPERSION-MANAGED SOLITONS

In this Section, we consider the dynamics of the DMS in our recirculating loop experiment. Our focus is on determining the requirements for an initial pulse to reach a steady state in which it varies periodically during one round-trip through the recirculating loop and on describing both the initial transient and the final steady-state evolution. We have found through careful comparison of theory and experiment that gain saturation in the amplifiers plays a critical role in our experiments, while third-order dispersion and saturable absorption, due to, for example, nonlinear polarization rotation, do not. It is our view that the modeling approach presented here—particularly our model of gain saturation—will have a wider range of applicability than to just our experiments. In order to concentrate on the dynamics of the DMS pulse, we set the ASE noise to zero in the investigations of this section. We also set the third-order dispersion and the saturable absorption to zero in most of this section, except near the end where we examine their importance.

We first consider the impact of gain saturation on the initial transient evolution of the input pulses. Fig. 2 shows the evolution of a set of initially Gaussian-shaped pulses at the output port of the recirculating loop when $G_0 = 32.45$ dB with$G_{a,0} = 5.4$ dB and $G_{b,0} = 10.85$ dB, while the average dispersion $D_{\rm av}$ equals 0.02 ps/nm–km. We see that they undergo a transient evolution over about 5000 km before settling down into a periodically stationary state. We also see that the evolution is apparently identical for all the pulses regardless of where they fall in the pulse stream. Thus, nearest neighbor interactions are negligible in this case, despite the stretching of the DMS pulses. Pulses that are initially hyperbolic-secant shaped undergo a nearly identical evolution as do a number of other pulse shapes. This re-

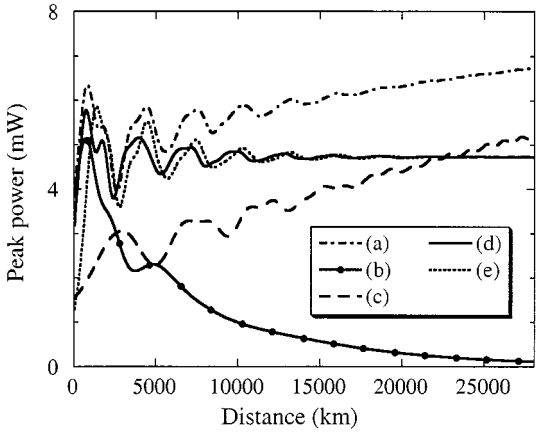

Fig. 3. The influence of different gain model to the stabilization of the DMS pulse propagation. (a) Without gain saturation, $G_0 = 31.6$ dB with $G_{a,0} = 5.0$ dB and $G_{b,0} = 11.6$ dB, and $P_{\rm in} = 9$ dBm. (b) Without gain saturation, $G_0 = 31.5$ dB with $G_{a,0} = 5.0$ dB and $G_{b,0} = 11.5$ dB, and $P_{\rm in} = 9$ dBm. (c) Without gain saturation, $G_0 = 31.6$ dB with $G_{a,0} = 5.0$ dB and $G_{b,0} = 11.6$ dB, and $P_{\rm in} = 5$ dBm. (d) With gain saturation, $G_0 = 32.45$ dB and $P_{\rm in} = 9$ dBm. (e) With gain saturation, $G_0 = 32.45$ dB and $P_{\rm in} = 5$ dBm. In cases (d) and (e), the values of $G_{a,0}$ and $G_{b,0}$ are the same as in Fig. 2.

sult is consistent with our experiments that indicate the DMS behavior is independent of the input parameters over a wide range [24]. This stability in the loop's behavior is a consequence of the gain saturation and the filtering. If the gain saturation is neglected, the initial pulse shapes that are launched into the system must be very close to the final periodically stationary pulse shapes in order for the system to converge; this sensitivity is in contradiction to the experiments. This point is illustrated in Fig. 3, in which we show the evolution of the peak power of a Gaussian-shaped pulse as we vary the round-trip gain G_0 and the peak power of the input pulse $P_{\rm in}$. In cases 3(a)–(c), in which the gain saturation is turned off, the system has difficulty stabilizing. In cases 3(a) and (c), the pulses are overamplified so that the amplitudes of the pulses continually increase and eventually blow up. In case 3(b), the pulses are underamplified and eventually disappear. By contrast, in cases 3(d) and (e), in which gain saturation is included, the pulses ultimately stabilize with the same pulse shape, regardless of the details of the input pulse shapes.

We next consider the detailed dynamics of the DMS pulse after the system has reached its steady state using the same set of parameters, as in Fig. 2. We used the first pulse in the pulse train shown in Fig. 2 to create Fig. 4 after verifying that the results did not depend on which pulse we used. The output average power nearly equals 0 dBm. These values produce results that correspond well to our experiments [24]. In Fig. 4(a), we directly compare the experimentally measured FWHM pulse durations to our simulation results at the taps shown in Fig. 1. Note that the horizontal scale is expanded in the anomalous dispersion regime for better visibility. Agreement between our experiments and our simulations is excellent. In Fig. 4(b) and (c), we show the variation of the pulse peak power and the chirp as a function of position along the loop. Here, we define the chirp as the second derivative of the phase with respect to time at the central position of the pulse in the time domain. Despite the asymmetric variation of the pulse peak power, the chirp goes nearly to zero

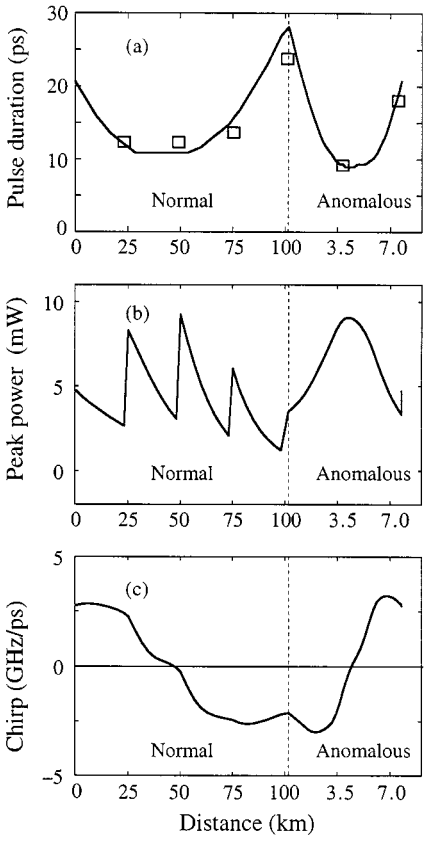

Fig. 4. The dynamics of the DMS signal at steady-state. We show the (a) duration; (b) peak power; and (c) the chirp of the pulse as functions of distance during one round trip in the loop. The squares show the experimentally measured the pulse durations.

at the midpoints of both the anomalous and normal dispersion spans just as in the lossless, unfiltered case [25]. The experimentally measured spectra and pulse durations are consistent with this result as we will show in Section IV.

In Fig. 5, we show the simulated behaviors of the pulse duration and the root-mean-square (rms) pulse bandwidth as $D_{\rm av}$ is changed. The pulse durations of the first and the last marks (ones) in the pulse train are calculated individually. The rms pulse bandwidth was calculated for the last (isolated) marks. The values of $G_{a,0}$ and $G_{b,0}$ are the same as in Fig. 2. When 0.02 ps/nm–km $< D_{\rm av} <$ 0.08 ps/nm–km, the minimum FWHM pulse durations only change by 1 to 2 ps. This small variation is below the resolution of our streak camera and is thus consistent with the conclusion from our experiments that the pulse dynamics were independent of $D_{\rm av}$ in this range [24]. However, the pulse bandwidth and the pulse-stretching factor increases as $D_{\rm av}$ decreases in the anomalous dispersion regime toward zero and the increases become very rapid when $D_{\rm av}$ is in the normal dispersion regime. The large stretching of the pulse durations in the normal regime occurs because the pulse energy is limited by the unsaturated gain G_0, so that the nonlinearity is not strong enough to support a normal DMS signal unless the stretching factor is large [26]–[30]. Comparing Fig. 5(a) to (b), we find that the large stretching in the normal dispersion regime leads to significant interpulse interactions. These interactions would be bad in a communication system.

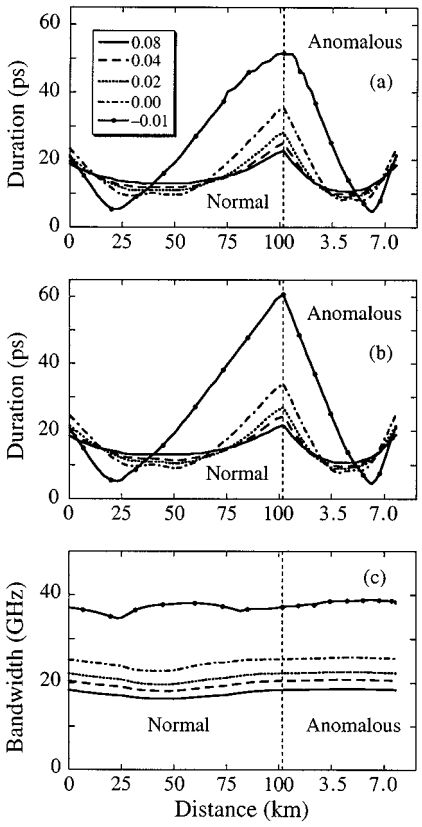

Fig. 5. Pulse dynamics with different path average dispersions. We show (a) the pulse duration of the first mark; (b) the pulse duration of the last mark; and (c) the root-mean-square pulse bandwidth of the last (isolated) mark as a function of distance during one round-trip in the loop.

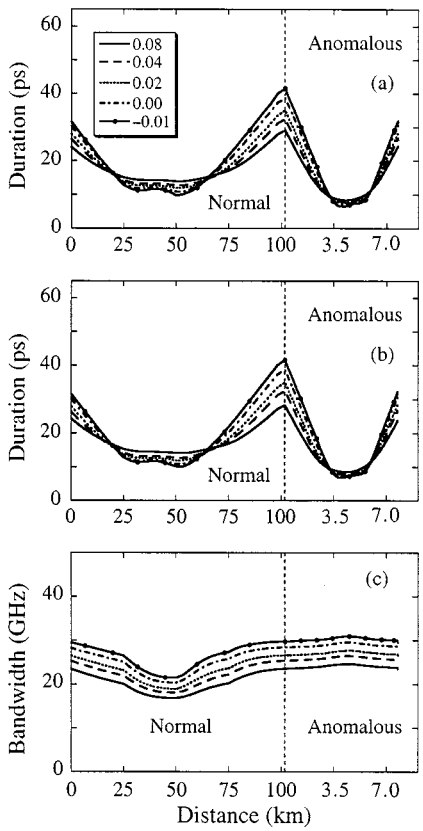

Fig. 6. Pulse dynamics with higher unsaturated gain G_0. We show (a), (b), and (c) as in Fig. 5.

By increasing the unsaturated gain G_0 to 34.45 dB, with $G_{a,0}$ and $G_{b,0}$ increased by 0.4 dB each, we observe a significant reduction in the stretching factor of the normal DMS pulses as shown in Fig. 6. The dynamical behaviors are identical for all the pulses inside the same pulse train, implying that there is no strong interpulse interaction in our system in this case.

We next considered the effect of nonzero third-order dispersion. Fig. 7 shows the propagation of a DMS in the loop with $D_{\rm av} = 0.02$ ps/nm–km and the same dispersion slope of 0.075 ps/nm^2–km as found in the fiber used in the experimental loop. All other parameters are the same as in Fig. 2. There is no visible change of the DMS dynamics with respect to Fig. 2, except that there is a slow constant drift of the pulse center with the pulse shape nearly unchanged. This effect occurs because the group velocity averaged over the bandwidth of the pulse is somewhat lower than the group velocity at the central frequency due to the third-order dispersion. This drift does not affect the system behavior because it is common to all the DMS pulses and will be removed by the clock recovery circuit. Similarly, simulations with $D_{\rm av} = 0$ ps/nm–km and $D_{\rm av} = -0.01$ ps/nm–km show that the dispersion slope of 0.075 ps/nm^2-km leads to no significant changes from the corresponding cases with zero dispersion slope.

Finally, we consider the effect of nonzero saturable absorption, which could be created for example by a combination of nonlinear polarization rotation and polarization-dependent loss [31], [32]. To include this effect, we add a saturable absorber

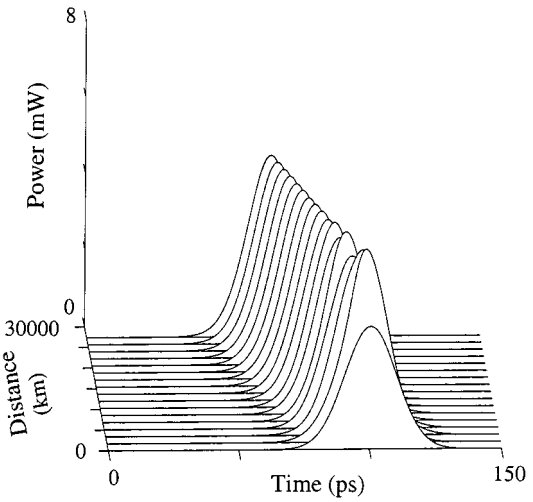

Fig. 7. Stable pulse propagation with third-order dispersion included in the simulation model.

after the optical bandpass filter. We modeled the saturable absorption as

$$q_{\rm out}(t) = q_{\rm in}(t)\left[1 - A\,\cos^2\left(\frac{|q_{\rm in}(t)|^2\pi}{2P_{\rm abs}}\right)\right]^{1/2}. \qquad (8)$$

We found that when the strength of the absorber—represented by A—is less than 0.4, there is no observable effect on the pulse dynamics. The value $A = 0.4$ corresponds to about a 0.1 dB loss difference between the pulse peak and the pulse tail per

round-trip in the loop when the threshold power of the saturable absorber $P_{\rm abs}$ is set to 50 mW. However, when A is larger than 0.4, which indicates a stronger saturable absorber, the loss difference between the pulse peak and the pulse tail is larger than 0.1 dB per loop. In this case, we saw that the pulse trains suffered serious distortion and could even drop during the propagation. No such effects were observed in our experiments [1]. Thus, we can conclude that under our operating conditions, the saturable absorption does not play a significant role in the DMS pulse dynamics.

IV. System Performance in the Presence of ASE Noise

ASE noise from the erbium-doped fiber amplifiers (EDFA's) degrades the marks (ones) by inducing timing jitter and amplitude jitter, as well as some pulse distortion; it also accumulates in the spaces (zeros). As we will show in the following, it is the noise increase in the spaces that limits the transmission distance in our recirculating loop.

The effect of the ASE noise is contained in the term $\hat{F}(z, t)$ in (1). We modeled its effects by adding noise in the Fourier domain after each amplifier. Writing the Fourier transform of $q(z, t)$ as $\tilde{q}(z, \omega)$ and using (5), we find that after the mth amplifier, we should add an amount of noise $\delta\tilde{q} = A\exp(i\varphi)$ to each Fourier component, where $A = [(G_m - 1)n_{\rm sp}n_2\hbar\omega^2 L_{\rm D}\Delta\nu/A_{\rm eff}T_0c]^{1/2}$, $G_m = \exp(\int_0^{L_{\rm amp}} 2g_m\,dz)$ is the gain associated with the mth amplifier, φ is a random phase uniformly distributed between 0 and 2π, and $\Delta\nu$ is the normalized bandwidth associated with each component. We set $n_{\rm sp} = 1.4$ to match the experimentally measured value. Strictly speaking, the real and imagery components of $\delta\tilde{q}$ are Gaussian-distributed with zero means and variances given by $A^2/2$. However, numerical experimentation has shown that using the approach described here leads to the same results since the correct amount of power is added on average to each Fourier component. Another issue is that we are using a scalar model and thus effectively neglecting the noise that is added in the polarization orthogonal to the signal polarization. This neglect is perfectly reasonable in standard soliton systems that are limited by spontaneous-signal beat noise—in particular, the timing jitter. However, as we will show, our system is limited by the growth of spontaneous–spontaneous beat noise in the spaces, and it is less evident that this neglect is justified. We have carried out careful experiments that show that when our system is operating optimally, the signal and noise are in fact copolarized through the combination of polarization-dependent loss and the polarization controller, thus justifying our neglect of the orthogonally polarized noise component. We will publish this investigation elsewhere. Anecdotal evidence indicates that this behavior is common in recirculating loop experiments that are less than 500 km in length, although no one to our knowledge has yet published a careful study of this issue.

In Fig. 8, we show the optical power of the 10-GHz radio frequency (RF) tone from our optical pulse train for both theory and experiment. The input signal is a 10 Gb/s pulse train. In our simulations, we used the 1-1-1-0-0-0-1-0 pulse pattern with

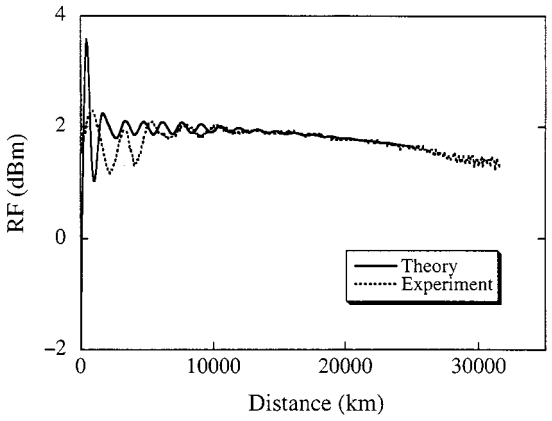

Fig. 8. The transient behavior of the 10-GHz RF component as a function of distance in the presence of the noise.

the initial pulse FWHM duration of 20 ps. The total unsaturated gain coefficient G_0 was set to 33.65 dB with $G_{a,0} = 5.8$ dB and $G_{b,0} = 10.45$ dB, which at $D_{\rm av} = 0.08$ ps/nm–km leads to the best agreement between theory and experiment. Initial oscillations, followed by a flat steady-state and a long-term degradation due to the accumulation of ASE noise, are all visible. The initial oscillations are due to variations in the pulse duration, and they arise from launching a nearly transform-limited pulse at the junction between the normal and anomalous regimes. At this junction, the pulse would have to have a significant chirp to avoid oscillations. The oscillations in theory and experiment are different. This difference occurs because the signal pulses from the laser source are slightly chirped in the experiment, and their shapes are somewhat different from ideal Gaussian shape that we assumed. Moreover, we expect that the gain coefficients and the actual amplifier relaxation time differ somewhat from the values we used. These quantities are difficult to measure accurately in practice. Nonetheless, the length of the transient regime and the behavior at steady state exhibit perfect agreement between theory and experiment. In Fig. 9, we show the pulse shape and the spectrum in the middle of the anomalous fiber section. Again, as also shown in Fig. 5(a), the minimum pulse duration is 9.7 ps in the simulation, while it was recorded as 9 ps in the experiment. The two values agree within the resolution of the streak camera. The spectrum is nearly Gaussian until about 30 dB down when the contribution of the ASE noise becomes evident. Thus, the experimentally measured spectra and pulse durations confirmed that the pulse is chirp-free at this point as predicted by the simulations shown in Fig. 4(c). Note the excellent agreement of the experiment and the simulations even at this level.

We next compare our simulation results to those obtained in [1]. As in [1], we consider two average dispersions, setting $D_{\rm av} = 0.04$ ps/nm–km and $D_{\rm av} = 0.08$ ps/nm–km. We set G_0 at different values in these two cases in order to keep the output-pulse average power at nearly 0 dBm, as in the experiment. Fig. 10 shows the signal intensity and both the experimentally and numerically determined eye diagrams at the input, while Fig. 11 shows the results after 24 500 km of propagation. The parameters for this set of simulations are as in Fig. 8. The simulations include an electrical fifth-order Bessel filter with a

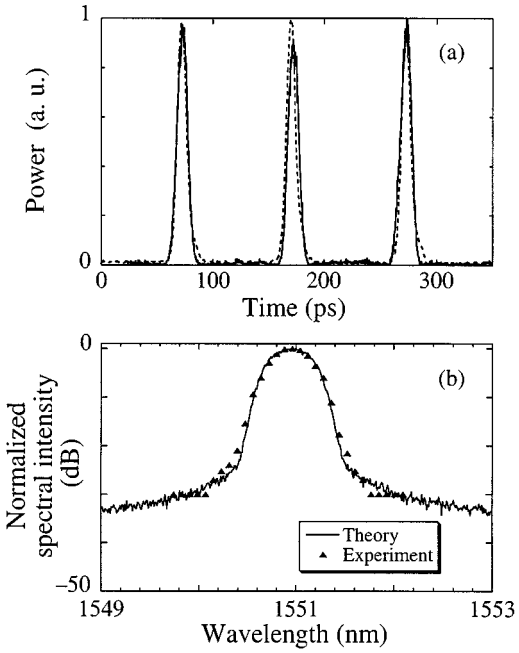

Fig. 9. The pulse shape at steady state in the presence of ASE noise. We show the (a) time, and (b) frequency variations. In (a), solid lines correspond to theory and the dashed lines to experiment. The simulated pulse shape in the time domain corresponds to the first three marks in our pulse pattern, while the experimental data is a group of three pulses that we measured using a streak camera. The simulated pulse spectrum corresponds to the last (isolated) mark in the pulse train averaged over 50 realization.

low-pass bandwidth of 4.3 GHz to match the experimental receiver. Including the electrical filter is critical in order to obtain good agreement between the eye diagrams and the BER's. The eye diagrams in Figs. 10 and 11 show the excellent agreements between the experiments and the simulations. We find a significant buildup of ASE noise in the spaces at 24 500 km, as well as significant change in the DMS pulses due primarily to amplitude jitter and timing jitter. It is the buildup of ASE noise in the spaces that limits our system.

We first consider the timing jitter [33]. To calculate it, we define the central pulse time position t_p [10] as

$$t_p = \frac{1}{U}\int_{-\infty}^{\infty} t|q(t)|^2\,dt \tag{9}$$

where $U = \int_{-\infty}^{\infty}|q(t)|^2\,dt$ is the pulse energy. The timing jitter is defined as

$$\delta t = [\langle t_p^2\rangle - \langle t_p\rangle^2]^{1/2}. \tag{10}$$

Using (10), we calculated the timing jitter using 100 different realizations of the ASE noise for both $D_{\rm av} = 0.08$ ps/nm–km and $D_{\rm av} = 0.04$ ps/nm–km. We set $G_0 = 33.6$ dB with $G_{a,0} = 5.8$ dB and $G_{b,0} = 10.4$ dB for $D_{\rm av} = 0.08$ ps/nm–km, and we set $G_0 = 33.2$ dB with $G_{a,0} = 5.8$ dB and $G_{b,0} = 10.0$ dB for $D_{\rm av} = 0.04$ ps/nm–km. The results are shown in Fig. 12. The agreement between theory and experiment is good considering the 0.5 ps uncertainty in the measurements. As expected, the timing jitter is smaller for smaller values of $D_{\rm av}$. Note that the growth rate of the jitter is smaller than the standard Gordon–Haus rate ($\propto Z^{3/2}$) due to the addition of the optical

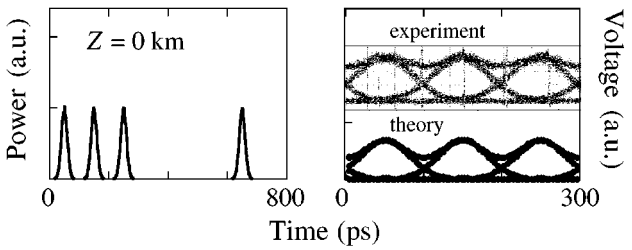

Fig. 10. Signal intensity and eye diagrams at the input. On the left, we show the numerically determined signal intensity in the optical domain, and the curves on the right show the eye diagrams after the electrical filter.

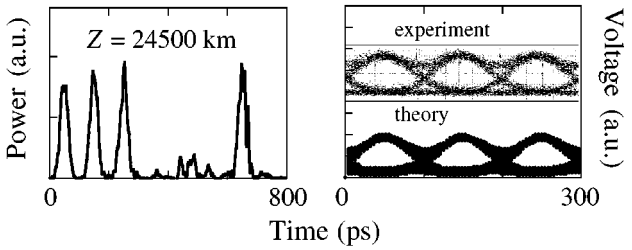

Fig. 11. The signal intensity and eye diagrams after 24 500 km. The curves are as in Fig. 10.

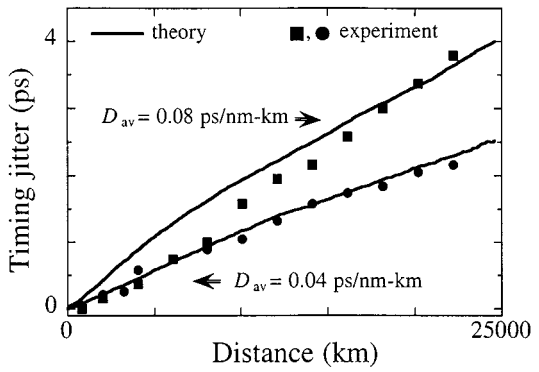

Fig. 12. Timing jitter as a function of the transmission distance.

filter [17], [33]–[37]. For our 10 Gb/s system we estimate that a timing jitter of 5.4 ps will lead to an error rate of 1×10^{-9}. Since the maximum timing jitter is well below 5.4 ps even with $D_{\rm av} = 0.08$ ps/nm–km, timing jitter does not limit our system.

The ASE noise also causes energy fluctuations in both the marks and spaces. Using our simulations, we calculated the mean and the variance of the optical energy in the marks and spaces. Assuming the fluctuation is Gaussian distributed in both the marks and spaces [38], we could then calculate the amplitude margin at a given error rate of 1×10^{-6}, which is the value we used in our experiments [1]. The margins are expressed as the voltage decision levels once the signal has passed through the receiver. While the error rate of 1×10^{-6} is higher than the standard values of 1×10^{-9}, it allowed us to experimentally collect a sizable number of errors in a reasonable time for this study. Moreover, with the increasing use of forward error correction, it is increasingly sensible to examine higher raw error rates. The assumption that the distribution of the marks and spaces about their means is Gaussian is also questionable. Indeed, this assumption is known to fail far out on the tails of the distribution

functions [38]. However, this assumption yields excellent agreement between the experiments and simulations, indicating that higher-order effects are not important at the error rates that we are considering.

Fig. 13 shows our comparison of the simulations and experiments when $D_{\rm av} = 0.08$ ps/nm–km and $D_{\rm av} = 0.04$ ps/nm–km. The only parameters that we changed are $G_0 = 33.65$ dB with $G_{a,0} = 5.8$ dB and $G_{b,0} = 10.45$ dB in first case and $G_0 = 33.3$ dB in the second case with $G_{a,0} = 5.8$ dB and $G_{b,0} = 10.1$ dB. The upper curves show the margin for the marks, and the lower curves show the margins for the spaces. Fig. 13 shows that while the margins for the marks undergo a slow, almost linear decay, the margins for the spaces grow nearly exponentially. This behavior is a well-known consequence of including a filter in the loop [39]. While the filter reduces timing and amplitude jitter, it also causes frequency-dependent loss. The DMS pulse has a finite bandwidth so that the net loss that it experiences due to the filter is determined by the integral of the loss over its bandwidth. This loss is compensated by the gain. By contrast, there are components of the spectrum in the spaces that experiences a net gain. Asymptotically, the growth of noise in the spaces may be written [34], [36]

$$H(z) = \frac{C}{\delta g(|\delta g'' z|)^{1/2}} \exp(2\delta g z) \tag{11}$$

and C is a constant coefficient that can be written approximately as

$$C = \sqrt{\pi} n_{\rm sp} \hbar \omega_0 \Gamma F(G) T_{\rm cal}/T_0 \tag{12}$$

where

$T_{\rm cal}$ is the time window size used in the simulation,
G is the actual gain coefficient, and
$F(G) = (G-1)^2/\{G[\ln(G)]^2\}$.

The quantity δg is the excess gain in the loop at the minimum loss point of the filter, and $\delta g''$ is the curvature of the filter at this point. The growth of the noise power for both the marks and spaces for the case $D_{\rm av} = 0.08$ ps/nm–km with the same parameters as in Fig. 13(a) is shown in Fig. 14. We assume that the noise power is proportional to the energy variance of the marks and spaces. We see that the noise growth in the marks is well fitted by a linear curve. In order to fit the growth in the spaces, we used a simplified z-dependent formula

$$H(z) = \kappa \exp(2\delta g z)/[\delta g z^{1/2}] \tag{13}$$

based on (11). By adjusting κ and δg, we found that the growth of the noise in the spaces is consistent with the nearly exponential growth given by (11). We thus conclude that the buildup of the ASE noise in the spaces limits the transmission distance in our system.

V. Conclusion

We have developed a model for nonlinear pulse propagation in an optical fiber transmission system with dispersion management that includes the effect of gain saturation in the EDFA's. We have carefully compared this model to recirculating loop experiments that we carried out in order to study the behavior of

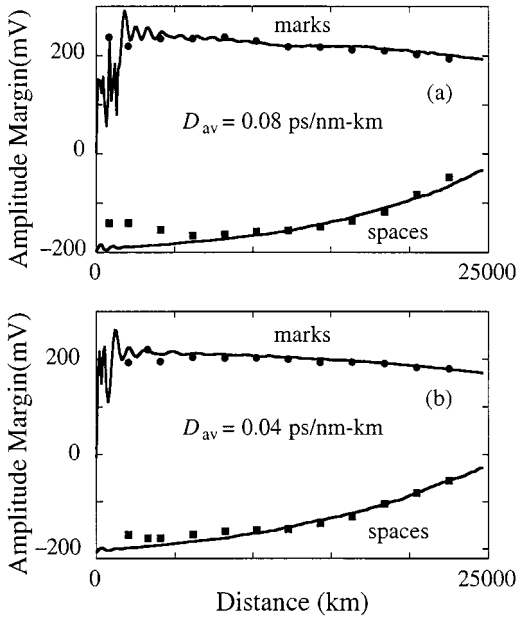

Fig. 13. Amplitude margin along the transmission line at a bit rate of 10 Gb/s. The upper curve shows the decision level of the marks, and the lower curve shows the decision level of the spaces. Squares and diamonds are the experimental data.

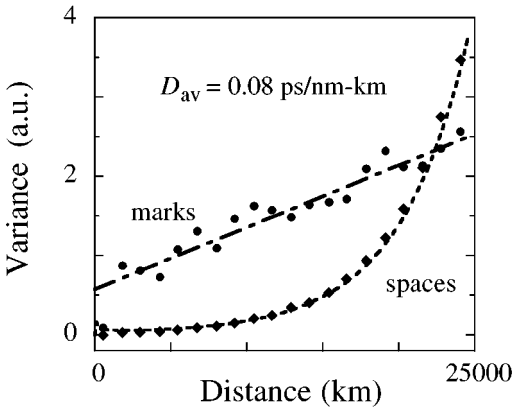

Fig. 14. Noise behavior in the system with $D_{\rm av} = 0.08$ ps/nm–km. The long dashed line shows a linear fit to the marks, and the short dashed line shows the fit to the spaces using (13).

DMS's. The simulations accurately matched the experimental data, yielding insights into the key physical effects and fundamental limitations on long-distance propagation in this system. We found that gain saturation in the EDFA's plays a key role in stabilizing the initial transient pulse evolution. By contrast, third-order dispersion and saturable absorption do not play a significant role. We accurately determined the steady-state dynamical evolution of the DMS's, and we found that the stretching factor increases dramatically as $D_{\rm av}$ reaches zero and becomes negative. The increased stretching factor leads to interpulse interactions that in turn limit the minimum $D_{\rm av}$ attainable. We then examined the accumulation of ASE noise and its impact on the behavior of the DMS's. We calculated the timing jitter for the DMS solitons in our system. We found excellent agreement with the experiments and showed that timing jitter does not limit the propagation distance. We then calculated the voltage mar-

gins, assuming a Gaussian distribution of the noise power, at an error rate of 10^{-6}, and we again found excellent agreement with the experiments. These results indicated that the principal limitation on the propagation distance in our system is the growth of amplified spontaneous emission noise in the spaces. We believe that our modeling approach will be of use for a wide array of systems—systems using RZ and NRZ—as well as systems using DMS.

ACKNOWLEDGMENT

One of the authors (C. R. Menyuk) would like to thank Prof. H. A. Haus for useful discussions concerning the copolarized noise.

REFERENCES

[1] J. M. Jacob and G. M. Carter, "Error-free transmission of dispersion-managed solitons at 10 Gbit/s over 24 500 km without frequency sliding," *Electron. Lett.*, vol. 33, no. 12, pp. 1128–1129, 1997.

[2] G. M. Carter, R.-M. Mu, V. S. Grigoryan, C. R. Menyuk, P. Sinha, T. F. Carruthers, M. L. Dennis, and I. N. Duling III, "Transmission of dispersion-managed soliton at 20 Gbit/s over 20 000 km," *Electron. Lett.*, vol. 35, no. 3, pp. 233–234, 1999.

[3] I. Morita, K. Tanaka, N. Edagawa, S. Yamamoto, and M. Suzuki, "40 Gbit/s single-channel soliton transmission over 8600 km using periodic dispersion compensation," *Electron. Lett.*, vol. 34, no. 19, pp. 1863–1865, 1998.

[4] J. M. Jacob, E. A. Golovchenko, A. N. Pilipetskii, G. M. Carter, and C. R. Menyuk, "Experimental demonstration of soliton transmission over 28 Mm using mostly normal dispersion fiber," *IEEE Photon. Technol. Lett.*, vol. 9, pp. 130–132, Jan. 1997.

[5] M. Nakazawa, Y. Kimura, K. Suzuki, H. Kubota, T. Komukai, E. Yamada, T. Sugawa, E. Yoshida, T. Yamamoto, T. Imai, A. Sahara, H. Nakazawa, O. Yamauchi, and M. Umezawa, "Field demonstration of soliton transmission at 10 Gbit/s over 2000 km in Tokyo metropolitan optical loop network," *Electron. Lett.*, vol. 31, no. 12, pp. 992–994, 1995.

[6] F. M. Knox, W. Forysiak, and N. J. Doran, "10-Gbit/s soliton communication systems over standard fiber at 1.55 μm and the use of dispersion compensation," *J. Lightwave Technol.*, vol. 13, pp. 1955–1962, Oct. 1995.

[7] G. M. Carter, J. M. Jacob, C. R. Menyuk, E. A. Golovchenko, and A. N. Pilipetskii, "Timing-jitter reduction for a dispersion-managed soliton system: Experimental evidence," *Opt. Lett.*, vol. 22, no. 8, pp. 513–515, 1997.

[8] N. J. Smith, F. M. Knox, N. J. Doran, K. J. Blow, and I. Bennion, "Enhanced power solitons in optical fibers with periodic dispersion management," *Electron. Lett.*, vol. 32, no. 22, pp. 54–55, 1996.

[9] M. Suzuki, I. Morita, N. Edagawa, S. Yamamoto, H. Taga, and S. Akiba, "Reduction of Gordon–Haus timing jitter by periodic dispersion compensation in soliton transmission," *Electron. Lett.*, vol. 31, no. 23, pp. 2027–2029, 1995.

[10] R.-M. Mu, V. S. Grigoryan, C. R. Menyuk, E. A. Golovchenko, and A. N. Pilipetskii, "Timing-jitter reduction in a dispersion-managed soliton system," *Opt. Lett.*, vol. 23, no. 12, pp. 930–932, 1998.

[11] E. A. Golovchenko, A. N. Pilipetskii, and C. R. Menyuk, "Periodic dispersion management in soliton wavelength-division multiplexing transmission with sliding filters," *Opt. Lett.*, vol. 22, no. 15, pp. 1156–1158, 1997.

[12] T. Yu, R.-M. Mu, V. S. Grigoryan, and C. R. Menyuk, "Energy enhancement of dispersion-managed solitons in optical fiber transmission systems with lumped amplifiers," *IEEE Photon. Technol. Lett.*, vol. 11, pp. 75–77, Jan. 1999.

[13] M. Matsumoto, "Theory of stretched-pulse transmission in dispersion-managed fibers," *Opt. Lett.*, vol. 22, no. 16, pp. 1238–1240, 1997.

[14] S. K. Turitsyn, "Theory of average pulse propagation in high-bit-rate optical transmission systems with strong dispersion management," *JETP Lett.*, vol. 65, no. 11, pp. 845–851, 1997.

[15] M. J. Ablowitz and G. Biondini, "Multiscale pulse dynamics in communication systems with strong dispersion management," *Opt. Lett.*, vol. 23, no. 21, pp. 1668–1670, 1998.

[16] D. Breuer, F. Küppers, A. Mattheus, E. G. Shapiro, I. Gabitov, and S. K. Turitsyn, "Symmetrical dispersion compensation for standard monomode-fiber-based communication systems with large amplifier spacing," *Opt. Lett.*, vol. 22, no. 13, pp. 982–984, 1997.

[17] S. Kumar, M. Wald, F. Lederer, and A. Hasegawa, "Soliton interaction in strongly dispersion-managed optical fibers," *Opt. Lett.*, vol. 23, no. 13, pp. 1019–1021, 1998.

[18] Y. Kodama, S. Kumar, and A. Maruta, "Chirped nonlinear pulse propagation in a dispersion-compensated system," *Opt. Lett.*, vol. 22, no. 22, pp. 1689–1691, 1997.

[19] M. Matsumoto, "Analysis of interaction between stretched pulses propagating in dispersion-managed fibers," *IEEE Photon. Technol. Lett.*, vol. 10, pp. 373–375, Mar. 1998.

[20] T.-S. Yang and W. L. Kath, "Analysis of enhanced-power solitons in dispersion-managed optical fibers," *Opt. Lett.*, vol. 22, no. 13, pp. 985–987, 1997.

[21] E. G. Shapiro and S. K. Turitsyn, "Theory of guiding center breathing soliton propagation in optical communication systems with strong dispersion management," *Opt. Lett.*, vol. 22, no. 20, pp. 1544–1546, 1997.

[22] C. R. Menyuk, "Application of multiple length scale methods to the study of optical fiber transmission," *J. Eng. Math.*, vol. 36, pp. 113–136, 1999.

[23] Corning data sheets for SMF-28 fiber and SMF-LS fiber.

[24] G. M. Carter and J. M. Jacob, "Dynamics of solitons in filtered dispersion-managed systems," *IEEE Photon. Technol. Lett.*, vol. 10, pp. 546–548, Apr. 1998.

[25] V. S. Grigoryan, T. Yu, E. A. Golovchenko, C. R. Menyuk, A. N. Pilipetskii, and C. R. Menyuk, "Dispersion-managed soliton dynamics," *Opt. Lett.*, vol. 22, no. 13, pp. 1609–1611, 1997.

[26] J. H. B. Nijhof, N. J. Doran, W. Forysiak, and F. M. Knox, "Stable soliton-like propagation in dispersion managed systems with net anomalous, zero and normal dispersion," *Electron. Lett.*, vol. 33, no. 20, pp. 1726–1727, 1997.

[27] V. S. Grigoryan and C. R. Menyuk, "Dispersion-managed solitons at normal average dispersion," *Opt. Lett.*, vol. 23, no. 8, pp. 609–611, 1998.

[28] S. K. Turitsyn and E. G. Shapiro, "Dispersion-managed solitons in optical amplifier transmission systems with zero average dispersion," *Opt. Lett.*, vol. 23, no. 9, pp. 682–684, 1998.

[29] J. N. Kutz and S. G. Evangelides, Jr., "Dispersion-managed breathers with average normal dispersion," *Opt. Lett.*, vol. 23, no. 9, pp. 685–687, 1998.

[30] A. Berntson, N. J. Doran, W. Forysiak, and J. H. B. Nijhof, "Power dependence of dispersion-managed solitons for anomalous, zero, and normal path-average dispersion," *Opt. Lett.*, vol. 23, no. 12, pp. 900–902, 1998.

[31] C.-J. Chen, P. K. A. Wai, and C. R. Menyuk, "Stability of passive mode-locked fiber lasers with fast saturable absorption," *Opt. Lett.*, vol. 19, no. 3, pp. 198–200, 1994.

[32] D. S. Govan, N. J. Smith, F. M. Knox, and N. J. Doran, "Stable propagation of solitons with increased energy through the combined action of dispersion management and periodic saturable absorption," *J. Opt. Soc. Amer. B*, vol. 14, no. 11, pp. 2960–2966, 1997.

[33] J. P. Gordon and H. A. Haus, "Random walk of coherently amplified solitons in optical fiber transmission," *Opt. Lett.*, vol. 11, no. 10, pp. 665–667, 1986.

[34] A. Mecozzi, "Long-distance soliton transmission with filtering," *J. Opt. Soc. Amer. B*, vol. 10, no. 12, pp. 2321–2330, 1993.

[35] Y. Kodama and A. Hasegawa, "Generation of asymptotically stable optical solitons and suppression of the Gordon–Haus effect," *Opt. Lett.*, vol. 17, no. 1, pp. 31–33, 1992.

[36] T. Georges and F. Favre, "Modulation, filtering, and initial phase control of interacting solitons," *J. Opt. Soc. Amer. B*, vol. 10, no. 10, pp. 1880–1889, 1993.

[37] N. J. Smith, W. Forysiak, and N. J. Doran, "Reduced Gordon–Haus jitter due to enhanced power solitons in strongly dispersion managed systems," *Electron. Lett.*, vol. 32, no. 22, pp. 2085–2086, 1996.

[38] D. Marcuse, "Derivation of analytical expressions for the bit-error probability in lightwave systems with optical amplifiers," *J. Lightwave Technol.*, vol. 8, pp. 1816–1823, Dec. 1990.

[39] L. F. Mollenauer, J. P. Gordon, and S. G. Evangelides, "The sliding-frequency guiding filter: An improved form of soliton jitter control," *Opt. Lett.*, vol. 17, no. 22, pp. 1575–1577, 1992.

R.-M. Mu, photograph and biography not available at the time of publication.

V. S. Grigoryan, photograph and biography not available at the time of publication.

Curtis R. Menyuk (S'88–F'98) was born March 26, 1954. He received the B.S. and M.S. degrees from Massachusetts Institute of Technology, Cambridge, in 1976 and the Ph.D. degree from the University of California, Los Angeles, in 1981.

He has worked as a Research Associate at the University of Maryland, College Park and at Science Applications International Corporation, McLean, VA. In 1986, he became an Associate Professor in the Department of Electrical Engineering at the University of Maryland Baltimore County, Baltimore, and he was the founding member of this department. In 1993, he was promoted to Professor. Currently, he is on sabbatical at the Laboratory for Telecommunications Sciences in Adelphi, MD. For the last few years, his primary research area has been theoretical and computational studies of fiber optic communications. He has authored or co-authored more than 120 archival journal publications as well as numerous other publications and has edited two books. The equations and computer algorithms that he invented to model the propagation of light in optical fibers have been cited in several textbooks and are used by industrial laboratories and in commercially available software throughout the world.

Dr. Menyuk is a member of APS and SIAM, and a fellow of OSA.

G. M. Carter (M'82–SM'85), photograph and biography not available at the time of publication.

J. M. Jacob photograph and biography not available at the time of publication.